Progress In Electromagnetics Research C, Vol. 129, 99–113, 2023

Systematic Flexible Antenna Performance Study of V-Folding Percentage Influence

Kishore A. K. Ayyala[1, *], Atul Thakur[1], Sahbi Baccar[2], Nour M. Murad[3], Mani S. Prasad[4], Preeti Thakur[5], Glauco Fontgalland[6], Yong Zhou[7], and Blaise Ravelo[7]

Abstract—In wireless technology, microstrip patch antennas are often used in communication systems with various designs. However, the effect of geometrically folded antennas on wireless communication performance is unclear. To address this problem, an in-depth study of the flexible antenna parameters was performed through V-folding analysis. A systematic and complete analysis of the percentage of folding in patch antennas was performed. The folding of patch antennas is expected to become mandatory because patch antennas are integrated and molded according to specified object shapes. The designed antenna was operated at 0.1–5.0 GHz to investigate the folding performance in the frequency range of 1.00–3.78 GHz used in many wireless applications, such as GPS, GSM, and LTE standards. A promising operating frequency for flat (unfold) antennas is 1.42 GHz with an achieved multiband bandwidth of 31.6 MHz, which shifted according to the folding angle 'a' but with good performance. The results of this study can be used to predict the performance of an antenna when it is placed on a product of any shape, according to the designed object pattern.

1. INTRODUCTION

To meet public and industrial needs, electronics and communication engineering are moving toward smart technologies, such as smart devices for healthcare, smart cities, smart homes, and smart cars [1–4]. In all aspects, wireless communication is required with different conformal structures [5, 6]. Among the different types of communication terminals, patch antennas (PAs) are the most useful for wireless communication because of their design simplicity and possible frequency bands [7–10]. Antenna design engineers are constantly seeking reliable antenna design solutions that can be integrated into future electronic and communication devices. According to different applications, antenna design with respect to the wearable device shape can be challenging [11–14]. Solutions involving flexible antennas have become a trend in antenna-design engineering. One of the greatest challenges in wireless communication is the choice of a flexible antenna with the best communication performance [13, 15–24]. Most bent antennas have proposed the use of textiles [19–22], Kapton, and other flexible materials. Innovative flexible antenna designs have been developed using different materials for different applications [15, 25, 26]. Recently, the study of electronics and antenna design on flexible substrates, such as polyethylene terephthalate (PET), Kapton [15–17], and paper [18], as a substrate has gained attention. Kapton [15–17] is one of the best low-cost polyimide film substrates for

Received 15 November 2022, Accepted 12 January 2023, Scheduled 29 January 2023

* Corresponding author: Kishore Ajay Kumar Ayyala (kishoreajay@gmail.com).

[1] Centre for Nanotechnology, Amity University, Haryana Gurgaon, India. [2] Electronics and Systems Department, Normandie University, UNIROUEN, ESIGELEC, IRSEEM Saint-Etienne-du-Rouvray, France. [3] PIMENT, Network and Telecom Lab, Institut Universitaire de Technlogie, University of La Reunion, Saint-Pierre 97410, France. [4] Amity Institute of Space Science & Technology, Amity University, Noida, India. [5] Department of Physics, Amity University, Haryana Gurgaon, India. [6] Federal University of Campina Grande, Applied Electromagnetic and Microwave Lab., Campina Grande/PB, 58429, Brazil. [7] School of Electronic and Information Engineering, NUIST, Nanjing, Jiangsu, China.

manufacturing aircraft, spacecraft, X-rays, 3D printing, flexible printed circuit boards (PCBs), and antennas. Moreover, Kapton [15–17] exhibits good insulation properties and extraordinary temperature stability. Kapton is compact, light, and has conformal design capabilities, including multiband and wideband performance [6, 18] in bent configurations.

Despite the increasing number of studies on flexible antennas [11–24], further research on design methods suitable for Internet-of-things objects integrated into communication systems for automobiles and devices is required. In this study, to improve the flexible antenna design, the effect of V-folding on antenna performance was investigated. Unlike previous studies [11–24], the present study focused on V-folded microstrip patch antennas (MPAs) initially designed by choosing the substrate working on different folding methods by different conducting patch structures holding good operating resonance frequency. A geometrical approach based on the influence of the percentage of folding (PF) on the flexible and deformable MPA performance was developed. Researchers studying antenna bending have reported that the change in MPA performance after folding may result from geometrical deformation [1, 2]. In the present study, another important method for changing the parameters by folding MPAs is introduced, which involves printing flexible MPAs on a Kapton substrate. This V-fold is unique in flexible patch antenna forming different conformal structures, but antenna molding on sharp edges will need V-folding analysis. The remainder of this paper is organized as follows. In Section 2, the MPA design method using a PF is explained. The proof-of-concept in this study was designed on a Kapton substrate. Section 3 focuses on the MPA 3D simulation results. The MPA performance with respect to the PF is also discussed. In Section 4, the MPA specifications are evaluated by assessing the gain, directivity, input impedance, and radiation efficiency based on previously reported theoretical considerations [27–30]. The validity of the MPA PF effect was studied by comparing the simulated and measured results, as discussed in Section 5. Finally, Section 6 concludes the article.

2. STRUCTURE OF FLEXIBLE MPA

This section focuses on the MPA design method. The proposed MPA proof-of-concept was designed using the commercial electromagnetic 3D simulator CST MWS 2018.

2.1. Flexible MPA Design Description

The flexible MPA, which was the main structure investigated in this study, had a $\lambda/2$ value, taking λ as the guided wavelength. As illustrated in Figure 1, it has a rectangular structure composed of metallic and dielectric bulk materials. This configuration was designed as a flat microstrip structure with a ground plane on the bottom side. A front view of the MPA proof of concept with a 35-µm-thick metallic copper part is shown in Figure 1.

In Figure 1, the dielectric Kapton substrate and metallic parts are represented in blue and yellow, respectively. The MPA was designed on a flexible Kapton substrate with length $L = 65.04$ mm and width $W = 80.9$ mm. The Kapton substrate had a dielectric constant $\epsilon_r = 3.4$ and thickness $h = 0.13$ mm. The key physical parameters L_p, W_p, W_i, b, c, d, and f_l corresponding to the metallic part were optimized to generate an MPA fundamental resonance frequency operating around $f_r = 1.42$ GHz in a flat horizontal position useful for mobile (aeronautical), radio astronomy, and meteorological satellite service. In the CST MWS design, the MPA was connected to a 50-Ω coaxial feed through an SMA connector.

The focus of this study was the V-geometrical shape-folding effect. In the following subsection, the geometric methodology of the parametrization of the folded MPA is described.

2.2. Definition and Representation Parameters of Flexible MPA V-Folding

Figure 2 shows a side view of a deformed flat MPA in a V-folded position designed using the CST MWS. This geometrically referenced representation of the flexible MPA is central to the V-folding analysis in this study. In this representation, the PF of the MPA can be controlled by the geometrical position of the transverse and horizontal folding axes. As shown in Figure 2, the V-folded structure is composed of a horizontal arm with physical length x from the connector and a folded arm with physical length d. The folding angle is 'a'.

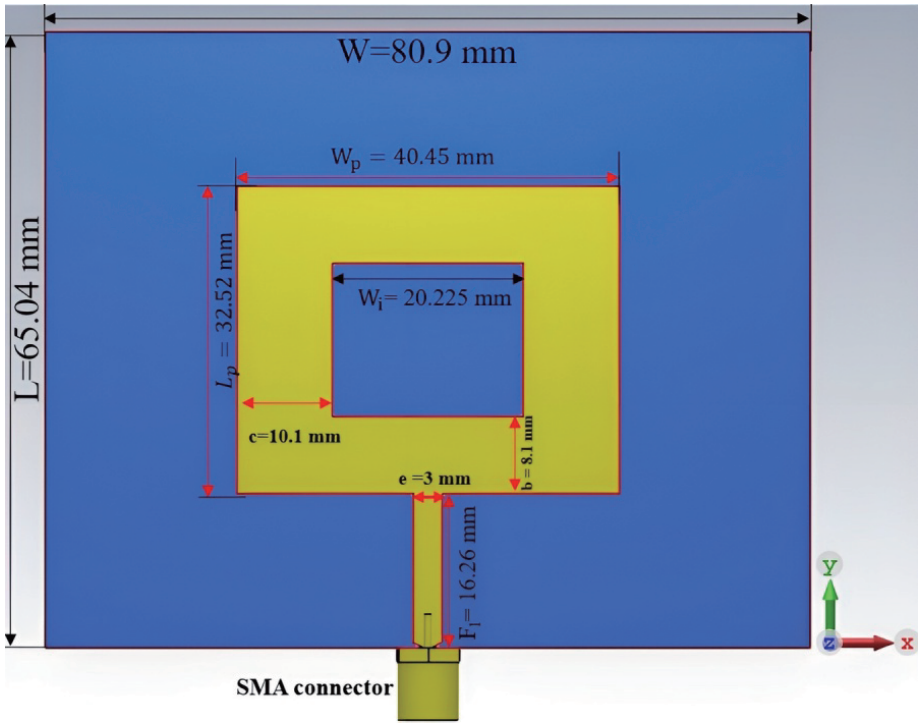

Figure 1. Front view with physical dimensions of the proposed CST MWS design of MPA in flat position.

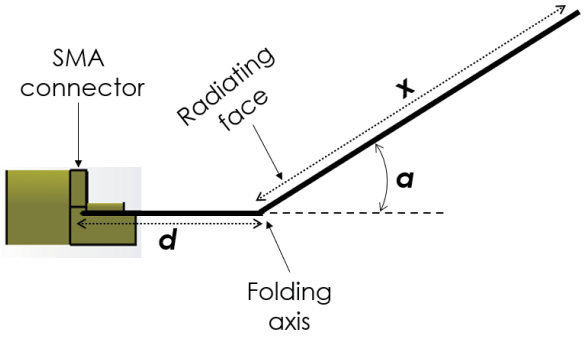

Figure 2. Side view of folded flexible MPA.

The folding effect on the MPA parameters was analyzed with respect to the partial lengths of d and $x = L - d$. The percentage of V-folding is a function of the ratio $d : L$, with $L = d + x$. The V-folding control parameter is defined as follows.

$$\mathrm{PF}(\%) = 100d/L \tag{1}$$

that calculates the increase and decrease in these physical lengths. It is assumed that the minimum value of PF is 10% because V-folding cannot be performed beyond that value owing to the coaxial feeding point. The V-folding side views for PF = 10% and 50% are shown in Figures 3(a) and 3(b), respectively. The corresponding perspective 3D views are illustrated in Figures 4(a) and 4(b), respectively.

Different design cases for the sample being considered are described in the next subsection.

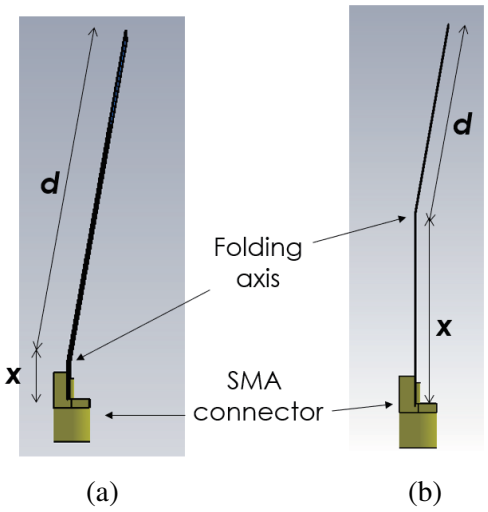

Figure 3. Side views of V-folded MPA for PFs of (a) 10% and (b) 50%.

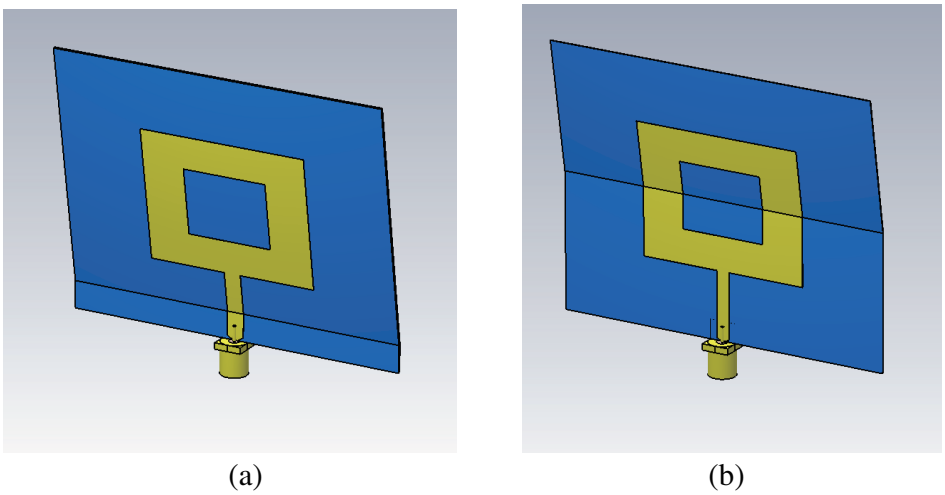

Figure 4. Three-dimensional views of folded MPAs for PFs of (a) 10% and (b) 50%.

2.3. Design Evolution Process with an Unfamiliar Folding Aspect

The present study focuses on the geometrical control of MPAs, as shown in Figure 2, to understand the influence of PF on antenna performance. For this purpose, MPA proofs of concept were developed based on PF, and samples for 37 positions under a flat condition are shown in Figures 5(a) and (b) according to Table 1.

The PF analysis focused on sharp edges folding on any objects or devices that have a V-shape, such as cars. The complete length of the MPA was $L = 65.04$ mm. When d is 10%, and x is 90%, the V-folding is at a point of exactly 6.504 mm, as shown in Figure 3. The PF starts at $d = 10\%$ and is increased for every additional 2.5 mm because the change in performance is observed at that increment, which inversely changes with x, as shown in Table 1. The computation time duration for CST 2018 is around 1.20 minutes for 8 threadings used.

The postprocessing used to interpret the CST MWS full-wave simulation sample results was performed using MATLAB.

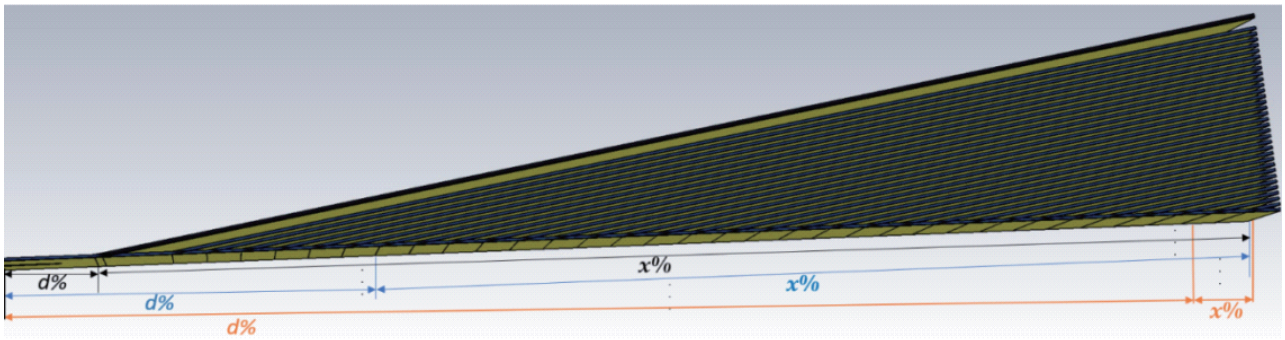

(a)

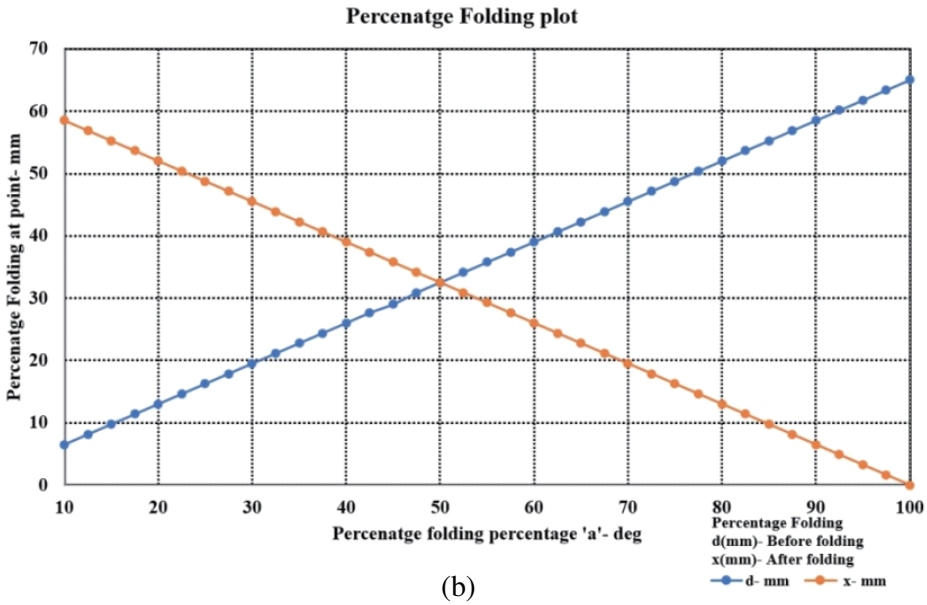

(b)

Figure 5. PF samples (a) Three-dimensional side view of combined MPA for different PF. (b) PF plots d and x according to Table 1.

3. POSTPROCESSING OF FULLWAVE SIMULATION RESULTS WITH RESPECT TO MPA V-FOLDING ANGLE

MPA V-folding results are discussed in this section. The main geometric parameters of the MPA structure were defined. Then, a basic analysis was performed to understand MPA behavior as a function of the folding parameter.

3.1. Equivalent Circuit

The MPA was folded and fixed at an angle of 'a' = 10° (V-shape) because Kapton folded beyond 10° does not have much variation. However, the complete length (L) is divided into d and x, resulting in combined percentage-wise folding. The MPA has an equivalent circuit consisting of lumped elements, such as a resistor, inductor, or capacitor, as shown in Figure 6. This equivalent circuit was designed in a schematic RF environment using a microwave circuit design and ADS simulator from Keysight Technologies. The change in geometrical shape affects x and L; therefore, the basic parameters of the MPA antenna are affected. The PF of the antenna changes from 10° to 100° will impact changes in the resistance, inductance, and capacitance values in the schematic shown reason for a change in basic parameters.

Table 1. PF of simulated MPA in detail with a folding point.

S no.	PF (%)	d (mm)	1-PF (%)	x (mm)	S no.	PF (%)	d (mm)	1-PF (%)	x (mm)
1	10	6.504	90	58.536	20	57.5	37.398	42.5	27.642
2	12.5	8.13	87.5	56.91	21	60	39.024	40	26.016
3	15	9.756	85	55.284	22	62.5	40.65	37.5	24.39
4	17.5	11.382	82.5	53.658	23	65	42.276	35	22.764
5	20	13.008	80	52.032	24	67.5	43.902	32.5	21.138
6	22.5	14.634	77.5	50.406	25	70	45.528	30	19.512
7	25	16.26	75	48.78	26	72.5	47.154	27.5	17.886
8	27.5	17.886	72.5	47.154	27	75	48.78	25	16.26
9	30	19.512	70	45.528	28	77.5	50.406	22.5	14.634
10	32.5	21.138	67.5	43.902	29	80	52.032	20	13.008
11	35	22.764	65	42.276	30	82.5	53.658	17.5	11.382
12	37.5	24.39	62.5	40.65	31	85	55.284	15	9.756
13	40	26.016	60	39.024	32	87.5	56.91	12.5	8.13
14	42.5	27.642	57.5	37.398	33	90	58.536	10	6.504
15	45	29.016	55	35.772	34	92.5	60.162	7.5	4.878
16	47.5	30.894	52.5	34.146	35	95	61.788	5	3.252
17	50	32.52	50	32.52	36	97.5	63.414	2.5	1.626
18	52.5	34.146	47.5	30.894	37	100 (Flat)	65.04	0	0
19	55	35.772	45	29.268	-	-	-	-	-

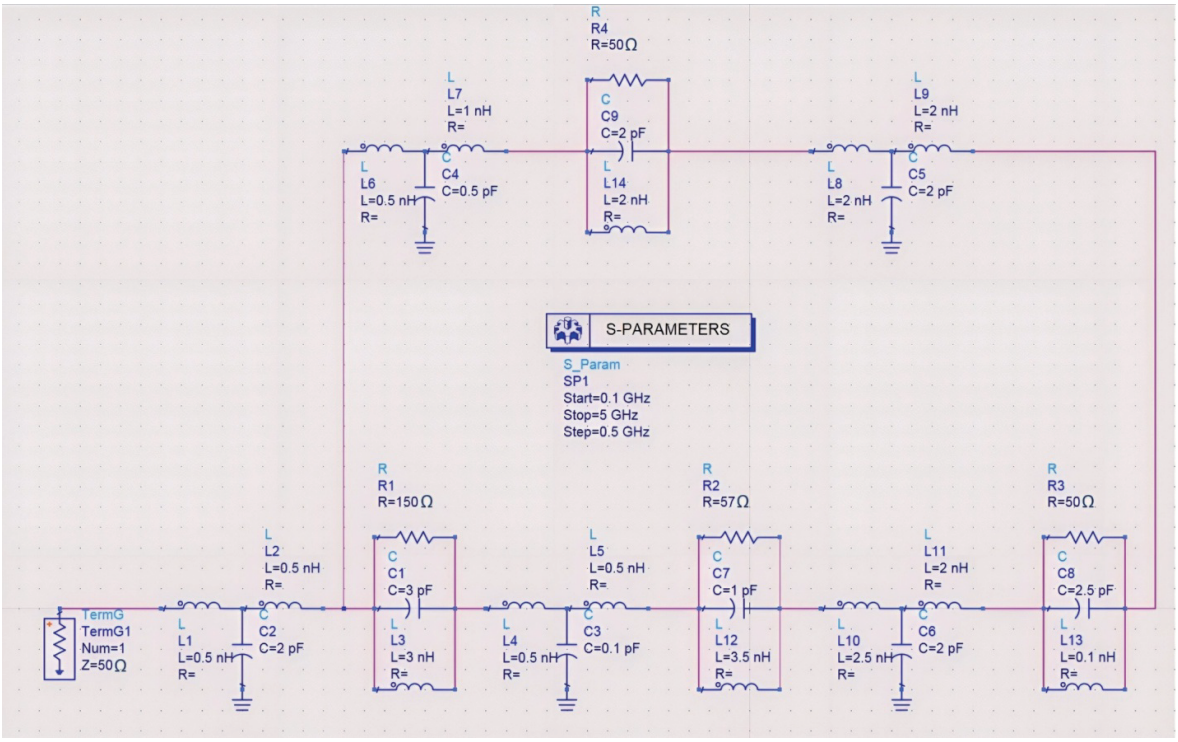

Figure 6. Flat MPA equivalent circuit designed in ADS schematic environment.

3.2. Analysis of Radiation Change Versus V-Folding Effect

The V-folding effect results from the radiation excited from a PA, as shown in Figure 2, before bending d and after x. In this study, the lengths d and x were first varied to monitor the performance with a fixed bend angle 'a' = 10° because folding a Kapton MPA from 0° to 10° was highly unstable; however, after 10°, it became stable at a certain angle. The PF performance shown in Table 2 was obtained after the simulation with CST MWS and considerable data processing. This unfamiliar influence of the MPA V-folding effect can be explained by the electric and magnetic fields radiated from the antenna with different cross-sections. As a result, the resonance frequency, radiation efficiency, directivity, and gain should change. The simulated results do not have any significant resonance frequency until $d = 37.5$ and $x = 62.5$ mm because folding MPA is not done on the patch (radiating). As shown in Table 2, the V-folding geometry affected the MPA performance.

Table 2. MPA specifications versus PF.

S no.	PF (%)	f_r (GHz)	S_{11} (dB)	Gain (dB)	Total efficiency (dB)	Directivity (dBi)
1	37.5	2.935	−11.77	−27.19	−30.89	3.401
2	40	2.76	−12.61	−29.25	−32.84	3.347
3	42.5	2.59	−10	−28.73	−32.91	3.713
4	45	1.47	−9.2	−21.35	−26.86	4.879
5	47.5	1.39	−10.02	−21.82	−26.86	4.589
6	50	1.31	−11.52	−22.39	−27.05	4.329
7	52.5	1.39	−10.02	−21.82	−26.86	4.589
8	55	1.18	−15.82	−23.97	−27.76	3.669
9	57.5	1.12	−18.71	−24.82	−28.23	3.352
10	60	1.02	−35.73	−26.40	−29.17	2.764
11	62.5	1.02	−29.09	−26.40	−29.18	2.772
12	65	3.39	−10.5	−27.02	−29.46	2.425
13	67.5	3.30	−11	−27.49	−29.74	2.236
14	70	3.21	−11.2	−27.89	−29.62	1.711
15	72.5	3.03	−12.03	−28.32	−30.86	2.471
16	75	1.42	−22.43	−18.26	−23.79	5.505
17	77.5	1.42	−24.26	−18.32	−23.85	5.518
18	80	1.42	−22.71	−18.40	−23.94	5.508
19	82.5	1.42	−22.62	−18.37	−23.94	5.542
20	85	1.42	−22.65	−18.38	−23.96	5.552
21	87.5	1.42	−22.98	−18.49	−24.05	5.529
22	90	1.42	−23.29	−18.51	−24.07	5.534
23	92.5	1.42	−22.62	−18.50	−24.07	5.544
24	95	1.42	−22.51	−18.50	−24.07	5.544
25	97.5	1.42	−23.02	−18.53	−24.10	5.551
26	100	1.42	−22.88	−18.54	−24.12	5.550

After the MATLAB analysis of the full-wave simulation results of each V-folded MPA sample, the antenna performance parameters resonance frequency (fr), gain, directivity, efficiency, and input impedance in Table 2 were obtained.

4. ANALYSIS AND DISCUSSION ON MPA SPECIFICATIONS WITH RESPECT TO PF

The analysis and interpretation of each MPA specification discussed in the previous section are elaborated in this section. This interpretation aims to understand the influence of V-folding on MPA performance.

4.1. Resonance Frequency

The resonance frequency is the frequency at which maximum power is delivered to the MPA. Analysis up to $f_{\max} = 5$ GHz shows that the MPA proof of concept has two resonance frequencies. The first represents the fundamental in the frequency band of 0.1–2.0 GHz, and the second represents the second harmonic in the frequency band of 2–5 GHz.

In this configuration, fr versus folding angle of the PF at more than 10° is plotted in Figure 7.

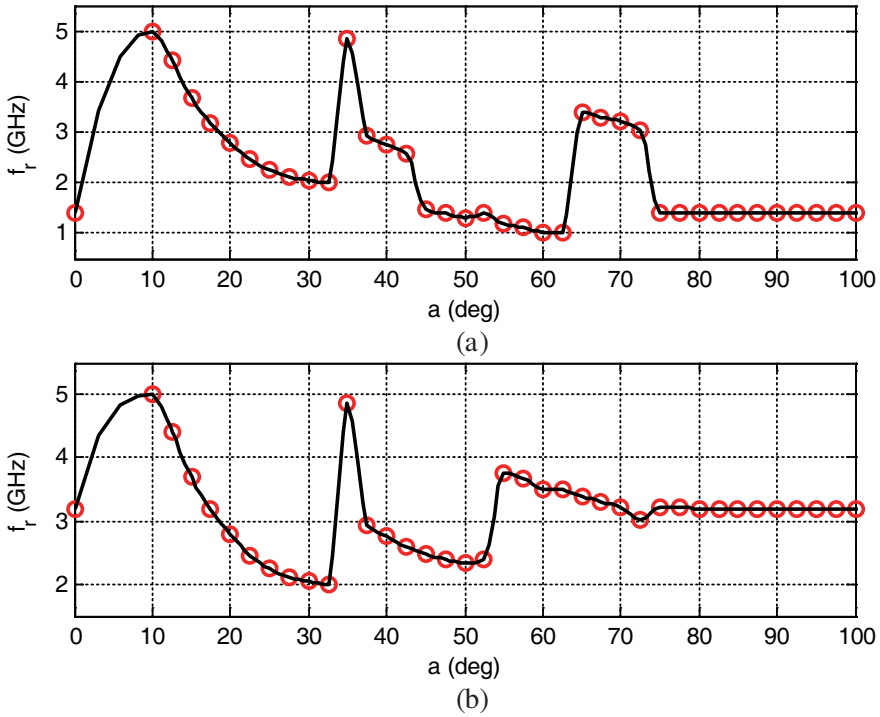

Figure 7. MPA resonance frequency versus folding angle 'a' in the (a) first and (b) second band.

For $a = 10°$–$35°$, the MPA did not achieve −10 dB. From 37.5° to 100°, the MPA operates with a multiband frequency, as shown in Figure 5(a). In the second band, −10 dB was achieved. As previously reported, fr shifts to the left or right depending on the substrate [5]. The best folding effect results of the PF occur at 60°–40°, as shown in Table 2, with multiband at approximately −35.73 dB. The resonance frequency shifts due to V-folding. There is a sharp bend of the antenna at a certain point, and the fringing field is affected due to the folding. While 10°–50° is treated as a lower folding angle 'a' has more shift due to the folding that occurs in conducting the patch, and it decreases later.

4.2. Gain

Figure 8 shows the results of the CST MWS simulations and the folding angle variation. The gain is another important parameter to be considered in antenna design engineering. Gain analysis by many researchers seeks to improve it using different approaches. In the present study, the gain varied when

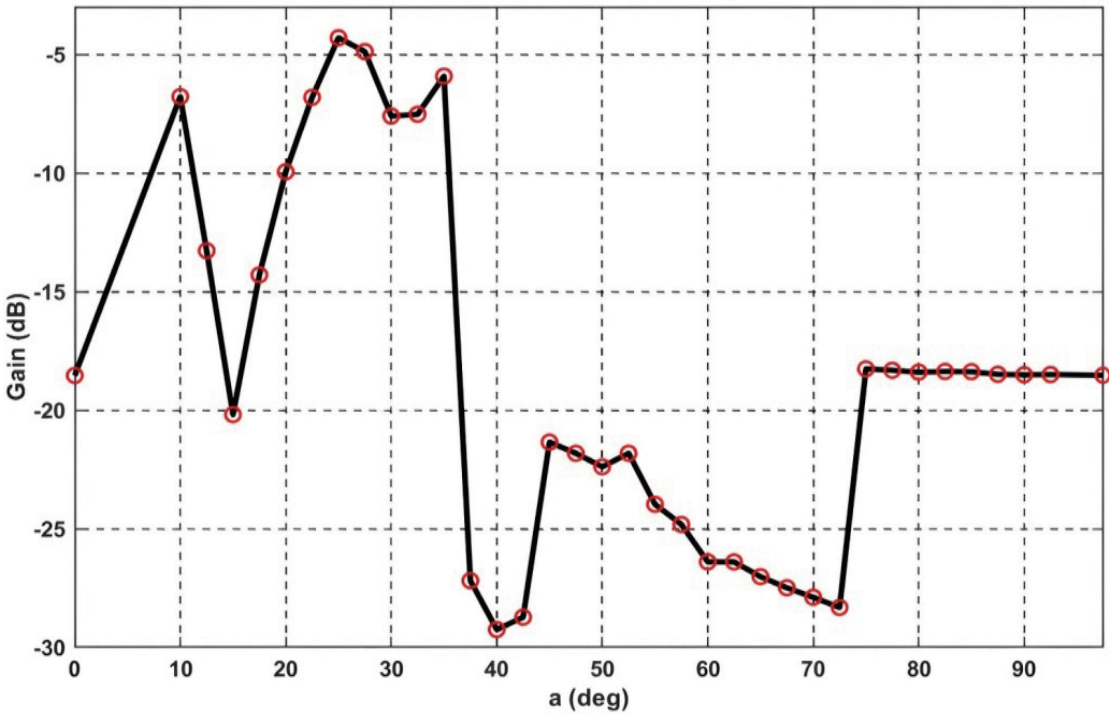

Figure 8. MPA gain versus 'a'.

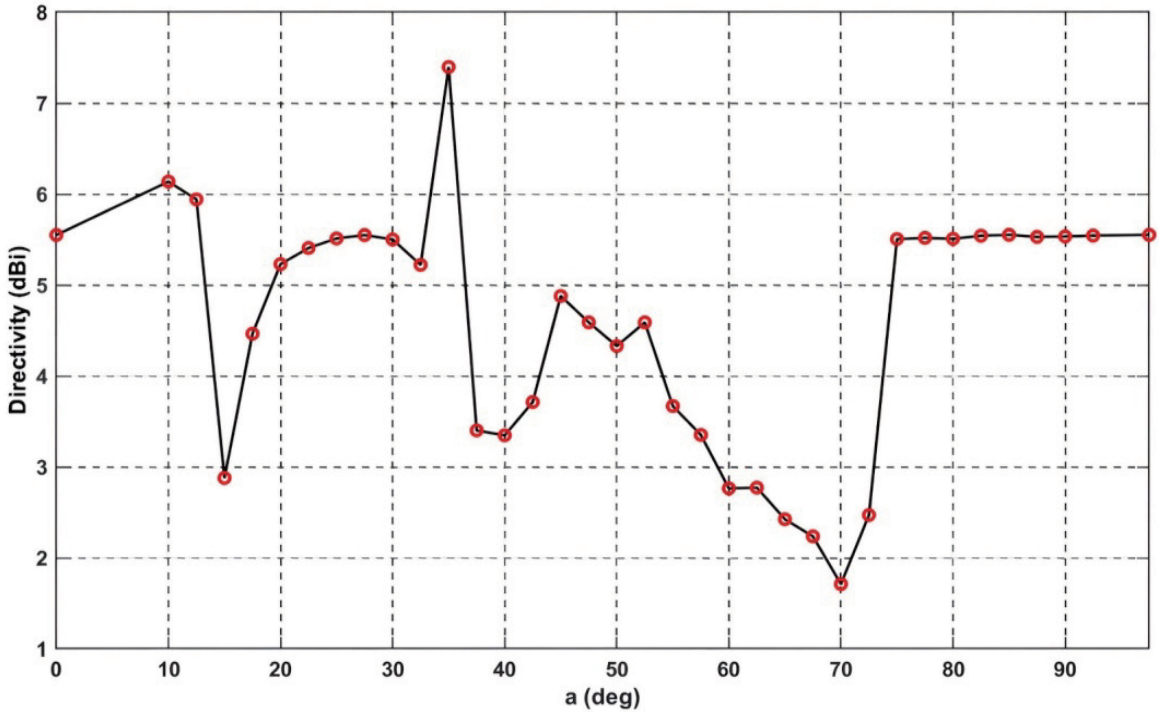

Figure 9. MPA directivity versus 'a'.

the folding percentage was in the range of 10°–35°. The gain varied particularly compared with the other PFs. The measured results were better than the simulated ones from 75° to 100°, achieving a 1.76 dB.

4.3. Directivity

Figure 9 highlights the behavior of the understudied MPA directivity. The results reveal the ability of the MPA to focus energy in a particular direction, as previously reported [6]. This figure shows that the directivity is constant when PF is between 75° and 100°. This is because the patch was not folded sufficiently, and there was no considerable effect on the equivalent circuit. The maximum directivity was 7.397 dB at 35°, owing to the bent patch edge. The measured results were better than the simulated ones.

4.4. Efficiency

Figure 10 shows the simulated maximum radiation efficiency of the developed MPA. The radiation efficiency parameter makes it possible to describe the efficiency of an antenna in transmitting and receiving RF signals. Radiation efficiency is defined as the ratio of the total power radiated by an antenna to the total input power received from the generator [7]. Figure 10 shows that the radiation efficiency is approximately −24.05 dB when the PF varies from 75° to 100°.

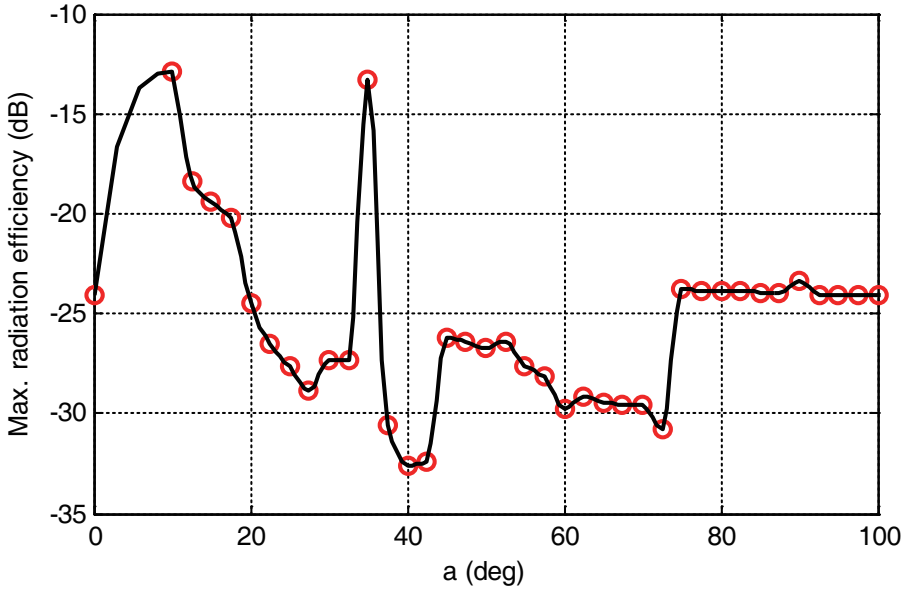

Figure 10. MPA maximal radiation efficiency versus 'a'.

However, the radiation efficiency was lower than −10 dB for the PF from 10° to 70°. This behavior is explained by the effect of V-folding, which appears mostly in the area outside the patch.

4.5. Input Impedance

Similar to flat MPAs, V-folded flexible MPAs operate under impedance matching, which is expressed by the input impedance. The real part of the antenna input impedance represents the power radiated or absorbed within the antenna. The imaginary part of the impedance represents the power stored near the antenna. The input impedance, Zin, of the proposed MPA can be expressed as $Zin = Rin + jXin$ by denoting Rin as the real part and Xin as the imaginary part representing the reactance. Figures 11(a) and (b) show Rin and Xin, respectively, versus the PF of the MPA in Figure 2.

Typical power antennas are non-radiated [8]. In the present case, the PF changed the input impedance of the MPA. The effect of V-folding on performance was less significant. As Figure 11 shows, a high resistance value compared with other PFs, approximately 89.5 Ω, and reactance of approximately 35.13 Ω at PF = 35° are achieved due to V-folding at the edge of conducting patch in 'b' represented in Figure 1.

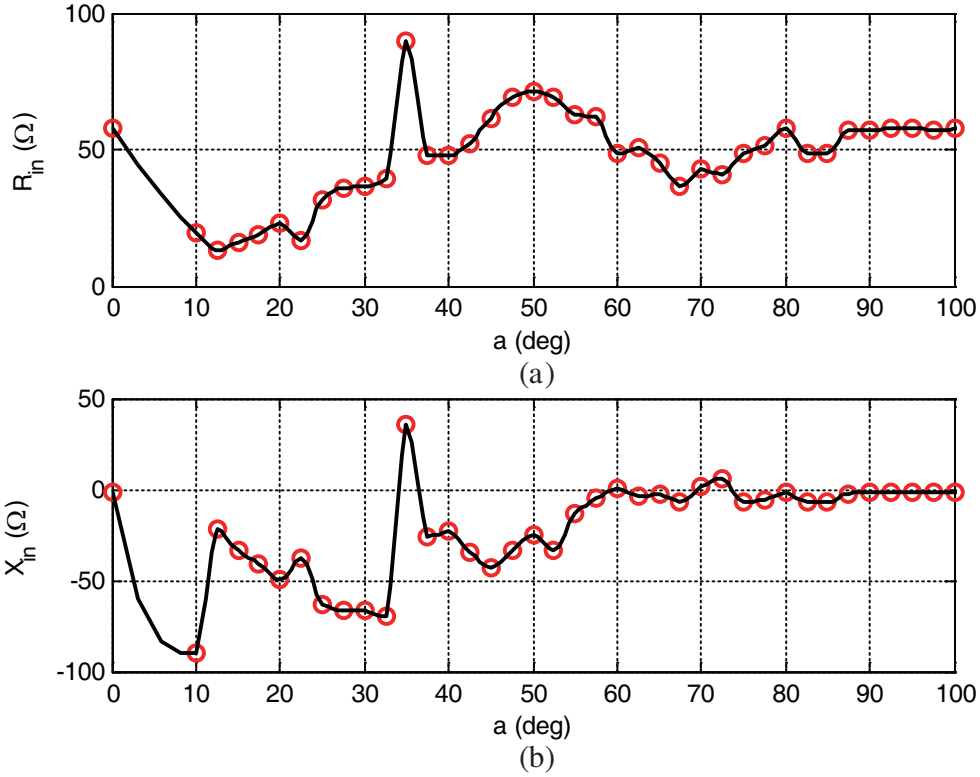

Figure 11. (a) Real and (b) imaginary parts of MPA input impedance versus 'a'.

5. EXPERIMENTAL INVESTIGATION OF V-FOLDED FLEXIBLE MPA

The experimental validation of the V-folding effect described in the previous section is discussed in Section 5. The empirical study was based on the measurement of a fabricated prototype of a flexible MPA, as shown in Figure 2.

5.1. Experimental Setup Description

The MPA was tested in an anechoic chamber of the electromagnetic research laboratory of the Central Research Facility of the Indian Institute of Technology Delhi. A photograph of the experimental environment with the MPA prototype placed on the test support is shown in Figure 12(a). Return loss was measured using an Anritsu MS2028C Vector Network Analyzer (VNA). The orientation of the tested MPA is shown in Figure 12(b). The folding aspect was controlled using a Polyvinyl chloride (PVC) fixture, as shown in Figure 12(c), with a thickness of 1.46 mm which does not affect performance. This PVC fixture was folded to 10° for the three PFs, as shown in Figure 13.

The PVC was folded in the required PF V-shape at an angle and placed on the back side so that it could hold the MPA according to the required shape and measure the results. Three MPA positions (PF = {25%, 40%, 77.5%}) are clearly shown in Figure 13. In the experimental setup, the fabricated MPA was presented with front and side views of every PF fixed on the PVC fixture to hold the designed antenna for extracting the measurement results.

5.2. Discussion of Simulated and Measured Result Comparison

The return loss, directivity, and gain of the tested prototype were extracted from the measurement results of the previous experiment. The resonance frequency was obtained from the return loss. Table 3 shows a comparison between the simulated and measured results versus the folding angle 'a'. The

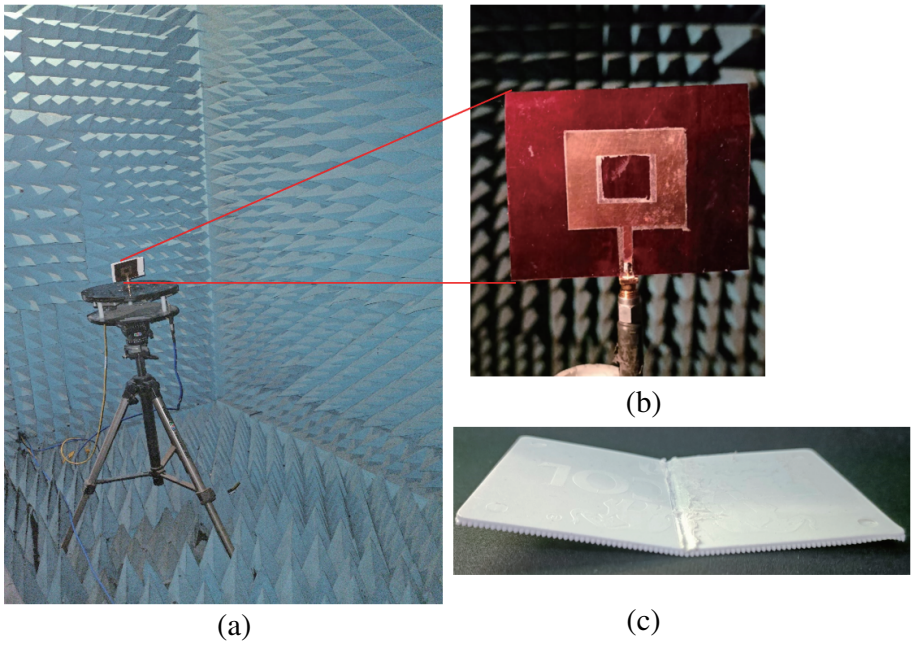

Figure 12. Photograph of anechoic chamber with folding MPA: (a) folded antenna in chamber, (b) flat antenna, and (c) PVC folded fixture.

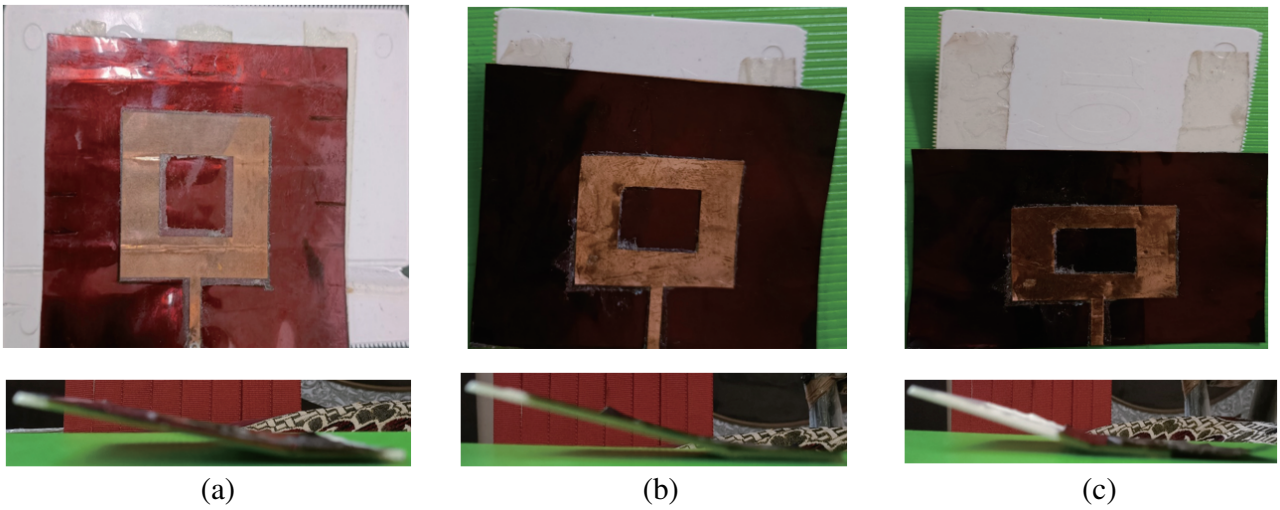

Figure 13. Illustration of control technique of MPA PF = (a) 25%, (b) 40%, and (c) 77.5% with side view (downside).

analytical model of the antenna yielded better results than the simulation. The parameters did not change before or after the folding of the flexible MPA. The measurement results are not close to the simulated ones due to the real-time behavior of the V-folding effect. The simulated results assorted for gain, directivity, and impedance have a small shift from PF of 50–70 around 0.4% fall due to the shift from the mid-point of the antenna towards the upper slab shown in Figure 1 causing an effect in fringing field and change in lumped elements (Figure 6). Once the PF reaches 72.5&75, it holds due to PF being conducted only on substrate apart from conducting patch.

The results of this study show the unique performance of V-folding at more than 10%, that is,

Table 3. Comparison results between simulation and measurements.

Approach	S no.	PF (%)	f_r (GHz)	S_{11} (dB)	Directivity (dBi)	Gain (dB)
Simulation	1	25	2.24	−4	3.015	−20.11
	2	40	2.76	−12.611	3.347	−29.25
	3	77.5	1.425	−24.263	5.518	−18.40
	4	100 (Flat)	1.42	−22.88	5.550	−18.54
Measurement	1	25	1.8	−21.51	4.74	−14.149
	2	40	1.7	−34.539	7.7815	−5.058
	3	77.5	1.4	−31.97	4.955	1.763
	4	100 (Flat)	1.729	−33.58	4.878	1.865

6.504-mm increments until 65.04 mm (100% flat position). The resonance frequency shifts for every slight change in the folding sample parameters. However, the gain and return losses of the analytical model were good (1.729 dB and −24.263 dB, respectively).

Planned future research includes the optimization of all parameters calculated with less folding effect and improved gain.

6. CONCLUSION

The folding effect of MPAs must be clearly understood when a perfectly conformal antenna is designed. In this study, a design method that considers geometrical deformation is developed. In addition, a method for analyzing the MPA antenna parameters was developed. Furthermore, behavioral changes in MPA performance were observed.

The folding effect was applied to a typical rectangular antenna fabricated using a flexible Kapton substrate. The influence of V-folding on the MPA performance was investigated through simulation. The essential parameters of the MPA proof-of-concept are return loss, directivity, gain, and radiation efficiency. The resonance frequency shifted beyond 10° for every folding sample, with only a slight change in the remaining parameters. However, the gain and return losses of the analytical model were good. Analysis of the simulation data showed that the antenna performance changed only when the radiator patch was folded but was stable when there was no folding on the patch, because the metallic surface patch was connected to the lumped circuit, as shown in Figure 6.

In future research, the V-folding MPA analysis result should be exploited to optimize the key parameters of the folded antenna through integrating it into complex geometrical wearable devices [12–14] by minimizing the folding effect and improving the gain, as well as to design and implement more general flexible PCBs for array antennas in different applications, such as energy harvesting, based on a previously introduced concept [31, 32].

7. DISCLOSURE STATEMENT

No potential conflict of interest is reported by the authors.

ACKNOWLEDGMENT

This work is supported by the Central Research Facility Indian Institute of Technology Delhi by providing an Anechoic chamber slot to measure the antenna performance. This research work was also supported in part by NSFC under Grant 61971230, in part by the Jiangsu Specially Appointed Professor program and Six Major Talents Summit of Jiangsu Province (2019-DZXX-022) and in part by the Start-up Foundation for Introducing Talent of NUIST.

REFERENCES

1. Bhuva, D., K. Sathashivan, A. Patil, et al., "Smart car systems: A need in smart city," *International Conference on Smart City and Emerging Technology (ICSCET)*, Vol. 1–3, 2018, DOI: 10.1109/ICSCET.2018.8537299.
2. Miranda, J., M. Memon, J. Cabral, et al., "Eye on patient care: Continuous health monitoring: Design and implementation of a wireless platform for healthcare applications," *IEEE Microw. Mag.*, 2017. Vol. 18, No. 2, 83–94.
3. Xu, Q., B. Wang, F. Zhang, et al., "Wireless AI in smart car: How smart a car can be?" *IEEE Access*, Vol. 8, 55091–55112, 2020.
4. Xu, G., Q. Zhang, B. Li, et al., "Smart car care systems and its technology prospects with service robots function," *IEEE International Conference on Information and Automation (ICIA)*, 1289–1294, 2014, DOI: 10.1109/ICInfA.2014.6932847.
5. Zhao, X. and J. Jin, "High gain directional antenna array for WiMAX application," *Trans. Tianjin Univ.*, Vol. 20, No. 5, 364–367, 2014.
6. Varma, R. and J. Ghosh, "Multi-band proximity coupled microstrip antenna for wireless applications," *Microw. Opt. Technol. Lett.*, Vol. 60, No. 2, 424–428, 2018.
7. Chen, H.-D., C.-Y.-D. Sim, J.-Y. Wu, et al., "Broadband high-gain microstrip array antennas for WiMAX base station," *IEEE Transactions on Antennas and Propagation*, Vol. 60, No. 8, 3977–3980, 2012.
8. Kumar, P. P. and R. Nakkeeran, "A new corrugated tooth like slot microstrip antenna for WiMAX/satellite applications," *Electrical Electronics and computer Science (SCEECS), 2014 IEEE Students' Conference*, 1–5, 2014.
9. Pandey, R. and D. K. Kumar Vishwakarma, "A fractalized meander-line EBG-based microstrip teeth-like patch slot antenna for use in satellite and defense applications," *Microw. Opt. Technol. Lett.*, Vol. 58, No. 8, 2010–2015, 2016.
10. Singh, A., M. Aneesh, and J. A. Ansari, "Analysis of microstrip line fed patch antenna for wireless communications," *Open Eng.*, Vol. 7, No. 1, 279–286, 2017.
11. Alharbi, S., R. M. Shubair, and A. Kiourti, "Flexible antennas for wearable applications: Recent advances and design challenges," *12th Eur. Conference on Antennas and Propagation (EuCAP)*, 1–3, 2018.
12. Song, L. and Y. Rahmat-Samii, "Patch antenna folding effects for wearable applications: Guidelines and design curves," *2018 United States National Committee of URSI National Radio Science Meeting (USNC-URSI NRSM)*, 1–2, 2018.
13. Song, L. and Y. Rahmat-Samii, "A systematic investigation of rectangular patch antenna bending effects for wearable applications," *IEEE Transactions on Antennas and Propagation*, Vol. 66, No. 5, 2219–2228, 2018, DOI: 10.1109/TAP.2018.2809469.
14. Froehle, P., T. Przybylski, C. McDonald, et al., "Flexible antenna for wireless body area network," *IEEE International Symposium on Antennas and Propagation & USNC/URSI National Radio Sci. Meeting*, 1214–1215, 2015.
15. Ahmed, S., F. A. Tahir, A. Shamim, et al., "A compact kapton-based inkjet-printed multiband antenna for flexible wireless devices," *IEEE Antennas and Wireless Propagation Letters*, Vol. 14, 1802–1805, 2015, DOI: 10.1109/LAWP.2015.2424681.
16. Rabobason, Y. G., G. P. Rigas, S. Swaisaenyakorn, et al., "Design and synthesis of flexible switching 1×2 antenna array on Kapton substrate," *Eur. Phys. J. Appl. Phys.*, Vol. 74, No. 3, 1–10, 2016.
17. Rabobason, Y. G., G. P. Rigas, S. Swaisaenyakorn, et al., "Design of flexible passive antenna array on Kapton substrate," *Progress In Electromagnetics Research C*, Vol. 63, 105–117, 2016.
18. Phan, H. P., T.-P. Vuong, P. Benech, et al., Study of bending effects of a wideband paper-based printed microstrip-fed antenna," *Microw. Opt. Technol. Lett.*, Vol. 62, No. 4, 1785–1794, 2020, DOI: 10.1002/mop.32233.
19. Boeykens, F., L. Vallozzi, and H. Rogier, "Cylindrical bending of deformable textile rectangular patch antennas," *Int. J. Antennas Propag.*, Vol. 2012, 1–11, 2012, DOI: 10.1155/2012/170420.

20. Mohandoss, S., S. K. Palaniswamy, R. R. Thipparaju, et al., "On the bending and time domain analysis of compact wideband flexible monopole antennas," *AEU Int. J. Electron. Commun.*, Vol. 101, 168–181, 2019, DOI: 10.1016/j.aeue.2019.01.015.
21. Kao, H.-L. and C.-H. Chuang, "Folding effects on a fabric-based antenna for wearable applications," *70th Electronic Components and Technology Conference (ECTC), IEEE Publications*, Vol. 2020, 1665–1670, 2020, DOI: 10.1109/ECTC32862.2020.00261.
22. Shafaet-Uz-Zaman, K. and M. A. Matin, "Analysis of folding and human body effects on sleeve-badge textile antenna performance," *TEQIP III Sponsored International Conference on Microwave Integrated Circuits, Photonics and Wireless Networks (IMICPW)*, Vol. 2019, 10–14, 2019, DOI: 10.1109/IMICPW.2019.8933267.
23. Ma, J., S. Li, and S. Zhang, "Folding effect on antenna with radiation performance for electronic tag," *Proc. 2014 3rd Asia-Pacific Conference on Antennas and Propagation*, Vols. 619–622, 2014, DOI: 10.1109/APCAP.2014.6992571.
24. Boyuan, M., J. Pan, E. Wang, et al., "Conformal bent dielectric resonator antennas with curving ground plane," *IEEE Trans. Antennas Propag.*, Vol. 67, No. 3, 1931–1936, March 2018, DOI: 10.1109/TAP.2018.2889146.
25. Simorangkir, R. B. V. B., Y. Yang, K. P. Esselle, et al., "A method to realize robust flexible electronically tunable antennas using polymer-embedded conductive fabric," *IEEE Trans. Antennas Propag.*, Vol. 66, No. 1, 50–58, 2018, DOI: 10.1109/TAP.2017.2772036.
26. Ibanez-Labiano, I., M. S. Ergoktas, C. Kocabas, et al., "Graphene-based soft wearable antennas," *Appl. Mater. Today*, Vol. 20, 2020, DOI: 10.1016/j.apmt.2020.100727.
27. Balanis, C., *Antenna Theory: Analysis and Design*, 3rd Edition, John Wiley & Sons, Inc., NJ, 2005.
28. Hammer, P., D. Van Bouchaute, D. Verschraeven, et al., "A model for calculating the radiation field of microstrip antennas," *IEEE Trans. Antennas Propag.*, Vol. 27, No. 2, 267–270, 1979, DOI: 10.1109/TAP.1979.1142054.
29. Aas, J. A. and K. Jakobsen, "Radiation patterns of rectangular microstrip antennas on finite ground planes," *12th Eur. Microwave Conference*, 384–389, 1982, DOI: 10.1109/EUMA.1982.333091.
30. Olaimat, M. M. and N. I. Dib, "Improved formulae for the resonant frequencies of triangular microstrip patch antennas," *Int. J. Electron*, Vol. 98, No. 3, 407–424, 2011, DOI: 10.1080/00207217.2010.547811.
31. Alex-Amor, A., Á. Palomares-Caballero, J. Moreno-Núñez, et al., "Ultrawideband inkjet-printed monopole antennas for energy harvesting application," *Microw. Opt. Technol. Lett.*, Vol. 63, No. 6, 1719–1726, 2021, DOI: 10.1002/mop.32803.
32. Murad, N. M., L. Rajaoarisoa, S. Lalléchère, et al., "Analysis of microstrip coupled line based data signal and energy hybrid receiver," *Journal of Electromagnetic Waves and Applications*, Vol. 34, No. 18, 2433–2454, 2020.